Available online at www.sciencedirect.com

ScienceDirect

Journal of the Franklin Institute 350 (2013) 3100–3115

Journal of The Franklin Institute

www.elsevier.com/locate/jfranklin

MTF estimation via BP neural networks and Markov model for space optical camera

Yingying Gu[a,b,*], Xiangheng Shen[a], Gengxian He[a]

[a]Changchun Institute of Optics, Fine Mechanics and Physics, Chinese Academy of Sciences, Changchun 130033, China
[b]University of Chinese Academy of Science, Beijing 100049, China

Received 11 January 2013; received in revised form 23 April 2013; accepted 27 June 2013
Available online 21 July 2013

Abstract

The modulation transfer function (MTF) is one of the essential criteria of space optical camera. However, the traditional measurement methods of MTF are limited by precise equipment and test site. In this paper, a novel method is proposed to estimate the MTF of space optical camera via BP neural networks and Markov model. Utilizing this method, the MTF of space optical camera can be estimated only from the images taken by the camera without additional measurement equipment. The principle is to use the information extracted from known MTF images to train a BP artificial neural networks (ANN), and then use the BP ANN to estimate the MTF of space optical camera from remote images. In the meanwhile, the Markov model is used to correct the results estimated by ANN. The experiment results show that the MTF estimation average relative error at Nyquist frequency can further narrow to 5% via BP neural networks and Markov model, compared with 9% using only BP ANN.

1. Introduction

The number of operating satellites is continuously increasing in recent decades, and more and more scientific and commercial communities become aware of the importance of satellites remote sensing in the area of agriculture industry, resources survey, disaster evaluation, etc. [1,2]. The space optical camera is one of the key payloads on satellites. It can be used to collect the optical information of interesting target by means of images.

*Corresponding author at: Changchun Institute of Optics, Fine Mechanics and Physics, Chinese Academy of Sciences, Changchun 130033, China. Tel.: +86 18686681605.
E-mail address: 18686681605@163.com (Y. Gu).

0016-0032/$32.00
http://dx.doi.org/10.1016/j.jfranklin.2013.06.024

In observation missions, it often needs to get the performance indexes of space optical camera, such as orbit altitude, ground resolution, swath, spectral bands and so on [3]. In addition to the routine indexes, it is useful to obtain the imaging performance of space optical camera [4–6]. There are many methods to access the imaging performance of space optical camera, including resolution test pattern method, spot diagram method, etc. However, the most universal and objective method accepted by researchers is MTF [7]. It can efficiently quantify the ability of a space optical system to transfer object contrast at a particular frequency. It has been widely used to characterize the imaging performance of space optical camera, such as the remote sensing satellites SPOT, GeoEye, SINA-1, etc. [3,8,9]. Meanwhile, the MTF is useful to focus space optical camera or to make a deconvolution filter, which purpose is to enhance image contrast [10].

There are several methods for measuring MTF, such as discrete or continuous frequency generation, image scanning, wavefront analysis, etc. [11,12]. However, the methods mentioned above have some disadvantages. Firstly, the precise test target is difficult to fabricate as space optical camera spatial resolution is increasing. Secondly, these methods need sophisticated equipment and are limited by the test site. The limitations of equipment and test site make the MTF test of space optical camera often before the launch. But it is not enough, the MTF may change due to vacuum in space, vibration during launch or change in material properties in time [13]. Therefore, new methods should be explored to measure the MTF of space optical camera without the above restrictions, either on ground assembly or working in orbit.

In this paper, a method is presented to estimate the MTF of space optical camera via BP neural networks and Markov model. Benefit from this approach, the MTF of space optical camera can be estimated from images taken by the camera, and it is not subject to precise measurement equipment and test site. The simulation method of images with controlled MTF and the extraction method of image characteristic parameters are presented in detail. And the basic principle of ANN designing is discussed. Finally, the Markovian prediction model is used to improve the accuracy of estimation result [14–16].

2. Background

2.1. Markovian jumping system

Markovian jumping system is a set of known subsystem models switching each other at a specific transition probability [17–19]. For discrete system, the jumping process $\{\gamma(k), k\geq 0\}$, taking values in a finite set $S\triangleq\{1, 2, 3, \ldots, s\}$, governs the switching among the different system modes. The system transition probabilities are defined as

$$P\{\gamma(k+1)=j|\gamma(k)=i\}=\pi_{ij} \tag{1}$$

where $\pi_{ij}\geq 0, \forall i, j\in S$, and $\sum_{j=1}^{s}\pi_{ij}=1$. Likewise, the transition probabilities matrix is defined as

$$\Pi=\begin{bmatrix}\pi_{11} & \pi_{12} & \ldots & \pi_{1s}\\ \pi_{21} & \pi_{22} & \ldots & \pi_{2s}\\ \vdots & \vdots & \ddots & \vdots\\ \pi_{s1} & \pi_{s2} & \ldots & \pi_{ss}\end{bmatrix} \tag{2}$$

However, the transition probabilities of many Markovian jumping system are partially unknown [20,21]. For instance, for a system with 4 operation modes, the probabilities matrix Π

may be defined as

$$\begin{bmatrix} ? & \pi_{12} & ? & \pi_{14} \\ ? & ? & ? & \pi_{24} \\ \pi_{31} & ? & \pi_{33} & ? \\ ? & ? & \pi_{43} & \pi_{44} \end{bmatrix} \tag{3}$$

where "?" represents the inaccessible elements. The general express of the transition probabilities was presented by Zhang for the first time [22,23]. For notational clarity, $\forall i \in S$, we denote $S = S_k^i + S_{uk}^i$ with $S_k^i \triangleq \{j : \pi_{ij} \text{ is known}\}$ and $S_{uk}^i \triangleq \{j : \pi_{ij} \text{ is unknown}\}$.

Moreover, if $S_k^i \neq \phi$, it is further described as

$$S_k^i = (k_1^i, \ldots, k_m^i) \quad \forall 1 \leq m \leq s \tag{4}$$

where $k_m^i \in N^+$ represent the mth known with the index k_m^i in the ith row of matrix π. Also, we denote $\pi_k^i = \sum_{j \in S_k^i} \pi_{ij}$. Moreover, if $S_{uk}^i = \phi$, the Markovian jumping system is the case with all-known transition probabilities. And if $S_k^i = \phi$, the Markovian jumping system is the case with all-unknown transition probabilities, the system is also named as switching system.

2.2. Modulation

The modulation of optical system is defined as [24]

$$M = \frac{I_{\max} - I_{\min}}{I_{\max} + I_{\min}} \tag{5}$$

where $I_{\max}$ is the maximum intensity produced by an image; $I_{\min}$ is the minimum intensity produced by an image.

Considering an optical signal at a spatial frequency υ given by Fig. 1, the light intensity can be described as

$$\begin{aligned} I(x) &= I_o + I_a \cos 2\pi\upsilon x \\ &= I_o\left(1 + \frac{2I_a}{2I_o} \cos 2\pi\upsilon x\right) \end{aligned}$$

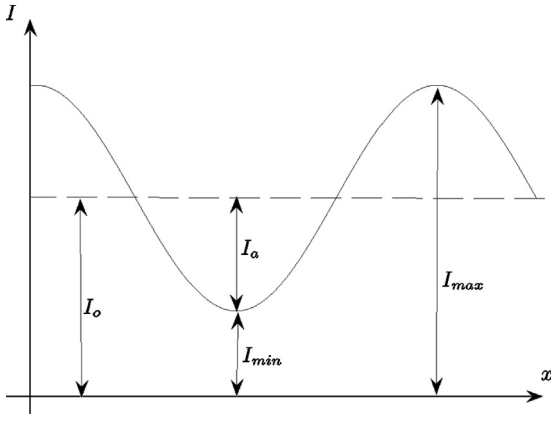

Fig. 1. Sinusoidal light intensity distribution.

$$= I_o\left(1 + \frac{I_{\max} - I_{\min}}{I_{\max} + I_{\min}} \cos\ 2\pi\upsilon x\right)$$

$$= I_o(1 + M\ \cos\ 2\pi\upsilon x) \tag{6}$$

Eq. (6) illustrates that the modulation M is the amplitude of sinusoidal light intensity loaded on the average light intensity I_o.

2.3. MTF

The MTF is the most widely used scientific method, which can characterize the imaging performance of space optical camera. It is a measure of the ability of an optical system to transfer various levels of detail from object to image. In other words, it characterizes how well the camera can reproduce the contrast of the observed target. Depending on the properties of space optical camera, the contrast of images reproduced by the optical system will decrease as the spatial frequency increased.

The MTF is defined as the ratio between the image modulation $M_i(v)$ and the object modulation $M_o(v)$ at a spatial frequency v

$$MTF(v) = \frac{M_i(v)}{M_o(v)} \tag{7}$$

In the meanwhile, the image within an isoplanatic patch can be represented as a convolution of a point spread function (PSF) over the scene

$$i_{mg}(x, y) = \int_{-\infty}^{+\infty}\int_{-\infty}^{+\infty} h(x-x', y-y')s_{cn}(x', y')\, dx'\, dy' \tag{8}$$

where $h(x, y)$ represents the spatial shape of PSF, and $h(x-x', y-y')$ represents a PSF at location (x', y') in image plane.

Each point in the scene radiates independently and produces a PSF in image plane with corresponding intensity and location. Mathematically, an image produced by optical system can be described by convolving the optical PSF over the scene. Since a convolution in space corresponds to a multiplication in frequency, the optical system can be seen as a spatial filter

$$I_{mg}(\xi, \eta) = H(\xi, \eta)S_{cn}(\xi, \eta) \tag{9}$$

where $I_{mg}(\xi, \eta)$ is the Fourier transform of image, $S_{cn}(\xi, \eta)$ is the Fourier transform of target scene, and $H(\xi, \eta)$ is the optical transfer function (OTF).

Obviously, the OTF is the Fourier transform of PSF. However, in order to keep the image intensity proportional to scene intensity, the OTF of optics is normalized by the total area under the PSF blur spot

$$H(\xi, \eta) = \frac{\int_{-\infty}^{+\infty}\int_{-\infty}^{+\infty} h(x, y)e^{-j\xi x}e^{-j\eta y}\, dx\, dy}{\int_{-\infty}^{+\infty} h(x, y)\, dx\, dy} \tag{10}$$

Finally, the MTF of optical system is $|H(\xi, \eta)|$.

3. Neural networks training set

3.1. MTF model of space optical camera

Generally, the space optical camera can be divided into three different scanning systems: whiskbroom imagers, pushbroom scanners, staring imagers [25]. In this paper, the MTF model of time delay and integration (TDI) charge-coupled device (CCD) space optical camera with pushbroom scanning system is discussed. It is composed of optics MTF, motion MTF, detector MTF and charge transfer MTF:

$$MTF = MTF_{optics} MTF_{motion} MTF_{detector} MTF_{charge} \tag{11}$$

Optics MTF is the MTF of the overall lens system. The optics MTF for a circular aperture is given by

$$MTF_{optics} = \begin{cases} \frac{2}{\pi}\left[\cos^{-1}\left(\frac{f_x}{f_{oco}}\right) - \frac{f_x}{f_{oco}}\sqrt{1-\left(\frac{f_x}{f_{oco}}\right)^2}\right], & \frac{f_x}{f_{oco}} < 1 \\ 0 & \text{elsewhere} \end{cases} \tag{12}$$

where f_x is the spatial frequency, $f_{oco} = D_0/\lambda$ is the optical cutoff, and D_0 is the aperture diameter.

The detector MTF is given by

$$MTF_{detector} = sinc(\pi \alpha f_x) \tag{13}$$

where $\alpha = a/F_{eff}$, a is the detector size, and F_{eff} is the effective focal length.

The linear motion MTF is given by

$$MTF_{motion} = sinc(Vt_i f_x) \tag{14}$$

where V is the image moving velocity on the image plane when space optical camera flew over a target on ground, and t_i is the integration time of TDI CCD.

Imperfect charge-transfer efficiency results charge-transfer MTF [24]

$$MTF_{charge} = \exp\{-n\varepsilon(1-\cos\ 2\pi f_x/f_c)\} \tag{15}$$

where ε is the charge-transfer inefficiency per transfer, n is the number of transfers in the CCD, and f_c is the clock frequency.

There are many MTF models of space optical camera in the literature [26–28]. In this paper, the model mentioned above will be used in our work.

3.2. Image simulations

Considering an image obtained by an optical system from a scene, the relationship between the scene and the image can be modeled as

$$g(x,y) = H[f(x,y)] + \eta(x,y) \tag{16}$$

where $g(x,y)$ is the image obtained by space optical camera, $f(x,y)$ is the scene, and $\eta(x,y)$ is the additive noise.

When imaging optical system is a linear shift-invariant system, the degraded image can be modeled in spatial domain by

$$g(x,y) = h(x,y) * f(x,y) + \eta(x,y) \tag{17}$$

where $h(x,y)$ is the degradation function represented in spatial domain, and the operator $*$ represents spatial convolution.

For processing convenience, Eq. (17) can be converted to frequency domain

$$G(u,v) = H(u,v)F(u,v) + N(u,v) \tag{18}$$

In spatial domain the degradation function $h(x,y)$ is known as PSF, and in frequency domain the degradation function $H(u,v)$ is known as OTF, which is mentioned in Section 2.3.

However, the model we discussed above is a continuous function model, but the realistic images obtained by the space optical camera are digital discrete, so in order to simulate the remote sensing images the model of sampled image is given by [28]

$$g(x,y) = [h(x,y)*f(x,y)]\sum_{i,j}\delta(x-j\Delta_x, y-i\Delta_y) + \eta(x,y) \tag{19}$$

where Δ_x and Δ_y are the sampling interval considered along the x and y directions. In frequency domain, Eq. (19) becomes

$$G(f_x,f_y) = \left[MTF(f_x,f_y)F(f_x,f_y)\right]*\sum_{i,j}\delta\left(f_x-\frac{j}{\Delta_x},f_y-\frac{j}{\Delta_y}\right) + N(f_x,f_y) \tag{20}$$

Using Eq. (20), the images with controlled MTF and noise can be simulated. In our practice, the image $f(x,y)$ should have sufficient sample rate compared with the simulated image. In our work, the image $f(x,y)$ is taken by a space optical camera (GeoEye) with a ground resolution of 0.5 m and a known MTF at Nyquist frequency. The simulated images have a ground resolution of 2 m and the MTF of images is under controlled. Some examples of simulated images with controlled MTF at Nyquist frequency are presented in Fig. 2.

4. Image characteristic parameters

4.1. Spatial spectrum vector

By the definition of MTF, when MTF is higher at a spatial frequency it means that the spatial frequency of the image is less attenuated by space optical camera. Therefore the spatial spectrum

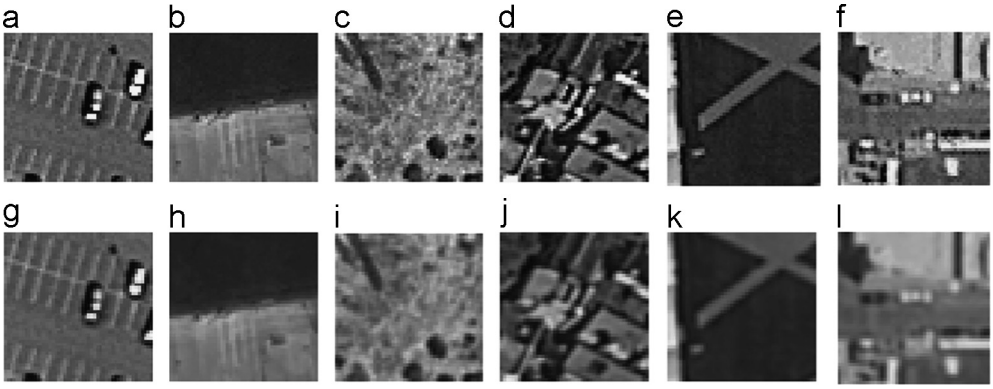

Fig. 2. Simulated remote sensing images with controlled MTF at Nyquist frequency.

vector given by Eq. (21) is selected as a parameter linked to the image MTF [29]

$$V(f) = \left[\sum_{v}|S(f,v)|; \sum_{u}|S(u,f)|\right] \tag{21}$$

where $S(\cdot)$ is the Fourier transform of images, $V(f)$ is the spectrum vector at spatial frequency f.

Fig. 3 shows four remote sensing images with different landscape structures and different MTF at Nyquist frequency. (a) and (b) of Fig. 3 are plain images with simple landscape structure. (c) and (d) of Fig. 3 are grove images with complex landscape structure. The spectrum vectors at Nyquist frequency of the four images are presented. And the Discrete Fourier transform of Fig. 3 is presented in Fig. 4.

Figs. 3 and 4 show that the spectrum vector decreases in directions x and y along with the MTF degradation for the same images (Fig. 3(a) and (b), (c) and (d)). It means that the spectrum vector is an effective parameter to characterize the MTF degradation. On the other hand, it can be concluded from Fig. 3 that the spectrum vector is also sensitive to the landscape structure of images. The images with complex landscape structures have a greater spectrum vector. So in order to estimate the MTF from the spectrum vector of images, the element of landscape

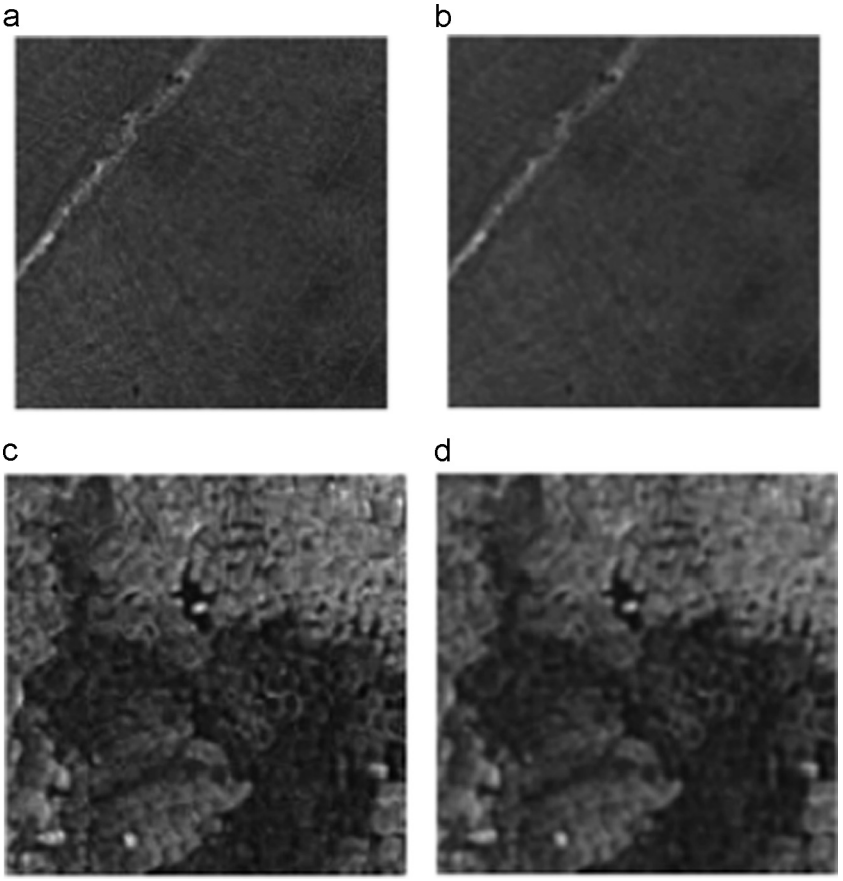

Fig. 3. The MTF and spectrum vector of different images. (a) MTF=0.45, $V(f_N)$=(41976,41076); (b) MTF=0.09, $V(f_N)$=(10848,9304); (c) MTF=0.45, $V(f_N)$=(60255,57305); (d) MTF=0.09, $V(f_N)$=(21993,23156).

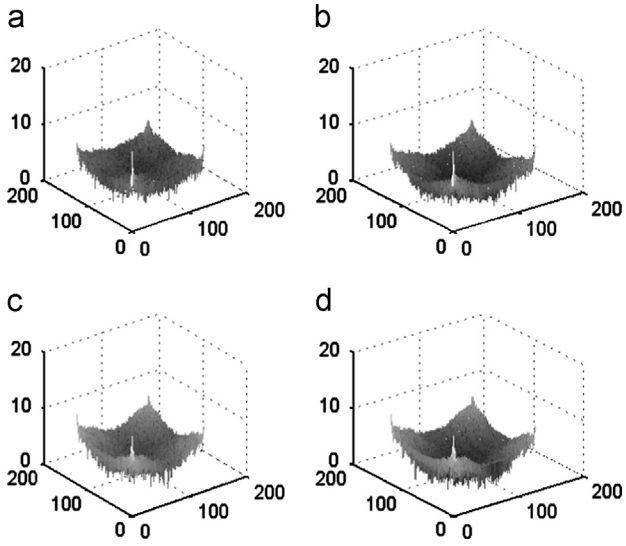

Fig. 4. Spectrum of plain and grove images when MTF=0.45 and MTF=0.09.

structure in images needs to be separated from the spectrum vector of images, this will be further discussed in Section 4.2.

4.2. Landscape structure parameters

In order to characterize the landscape structure of a remote sensing image, the notion of variogram is introduced [30,31]. It is often used for image processing [32,33]. The variogram $\gamma(h)$ of an image is a measurement of the average grey level variation of two points separated by a given number of pixels h.

For all pixels p of an image s,

$$\gamma(h) = \tfrac{1}{2}E\left[|s(p+h) - s(p)|^2\right] \tag{22}$$

where E is the statistical expectation.

In the meantime, the asymptote of variogram curve $\gamma(h)$ is the image variance. It can be inferred as

$$\begin{aligned}\gamma(h) &= \tfrac{1}{2}E\left[s^2(p) + s^2(p+h) - 2s(p)\cdot s(p+h)\right] \\ &= \tfrac{1}{2}E\left[s^2(p)\right] + \tfrac{1}{2}E\left[s^2(p+h)\right] - E\left[s(p)\cdot s(p+h)\right]\end{aligned} \tag{23}$$

when $h \to \infty$, $s(p)$ and $s(p+h)$ are mutual independent, so

$$E[s(p)\cdot s(p+h)] = E[s(p)]\cdot E[s(p+h)] \tag{24}$$

moreover, for all h there is a relationship between $E[s(p)]$ and $E[s(p+h)]$: $E[s(p)] = E[s(p+h)]$, so the asymptote of variogram curve can be inferred as

$$\lim_{h\to\infty}\gamma(h) = E[s^2(p)] - E^2[s(p)] = \sigma^2 \tag{25}$$

Fig. 5. Two images with different landscape structures.

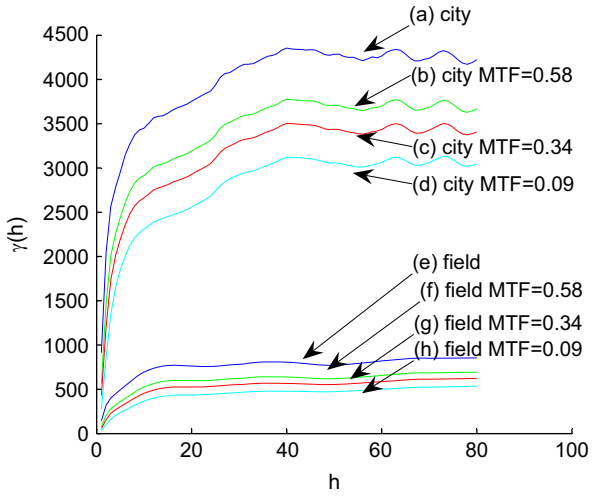

Fig. 6. Variogram curves of city and field images with different MTF.

In order to verify the effect of variogram to characterize the landscape structure of images, the variogram curves of two images with different landscape structures in Fig. 5 are shown in Fig. 6. It can be concluded that the variogram curves of these two images have their own characteristic shape, which are highly linked to the landscape structures of images. In other words, the shape of variogram curves is sensitive to the landscape structure of images. In the meantime, Fig. 6 illustrates that the variogram is not only sensitive to image landscape structure but also MTF. The variogram of two images decreases in y direction along with the MTF degradation at Nyquist frequency.

4.3. The statistical parameters

There are various statistical parameters of images such as mean, variance, skewness, kurtosis and so on. In practice, not all the statistical parameters of image should be selected as the neural

networks input. The basic rule is that the parameters which can entirely or partially characterize the MTF of images can be selected as the neural networks input. Unrelated parameters with MTF of images should be avoided in the neural networks. Otherwise it would be difficult to train the neural networks to reach satisfied estimation accuracy.

For example, mean and variance are two general statistical parameters in images. So we should confirm that which parameters can be selected as the neural networks input, it depends on the parameters and MTF are relevant. Fig. 7 shows the relationship between MTF and mean of city and field images. The mean varies along with the image scenery, but it cannot characterize the variation of MTF in images. That is to say the mean is not sensitive to MTF of images. Therefore the mean of images is not suitable for the neural networks input. However, Fig. 8 shows that variance of field and city images have a strong correlation with MTF of images. So the variance of images in our work can be accepted as the input parameters of the neural networks.

4.4. Quality index Q

4.4.1. Definition

Let $x=\{x_{ij}|i=1,2,\ldots,N \text{ and } j=1,2,\ldots,M\}$ and $y=\{y_{ij}|i=1,2,\ldots,N \text{ and } j=1,2,\ldots,M\}$ be the original image and degraded image respectively. The quality index Q is defined as

$$Q=\frac{4\sigma_{xy}\overline{x}\,\overline{y}}{(\sigma_x^2+\sigma_y^2)[\overline{x}^2+\overline{y}^2]} \tag{26}$$

where

$$\overline{x}=\frac{1}{NM}\sum_{i=1}^{N}\sum_{j=1}^{M}x_{ij},$$

$$\overline{y}=\frac{1}{NM}\sum_{i=1}^{N}\sum_{j=1}^{M}y_{ij},$$

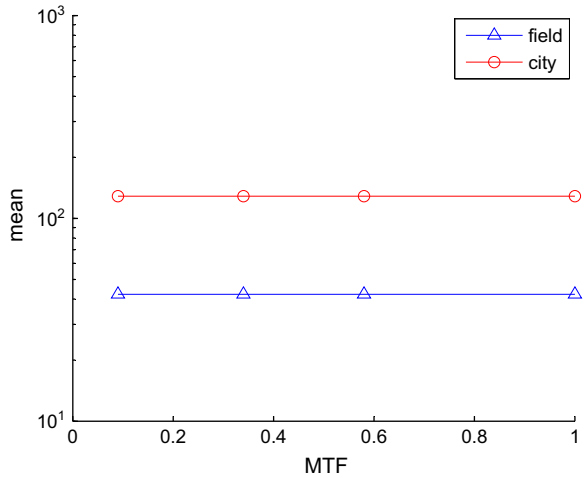

Fig. 7. Relationship between MTF and mean of city and field images.

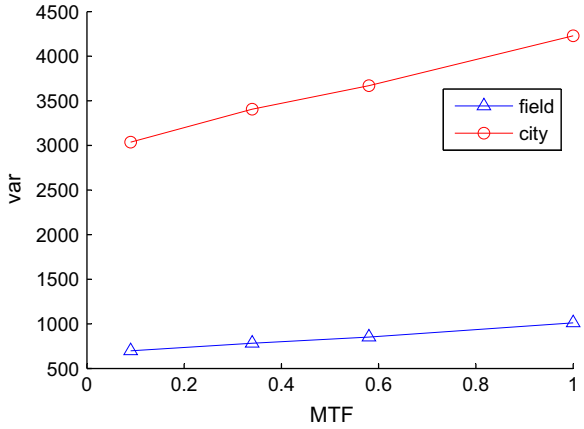

Fig. 8. Relationship between MTF and variance of city and field images.

$$\sigma_x^2 = \frac{1}{NM-1}\sum_{i=1}^{N}\sum_{j=1}^{M}(x_{ij}-\overline{x})^2,$$

$$\sigma_y^2 = \frac{1}{NM-1}\sum_{i=1}^{N}\sum_{j=1}^{M}(y_{ij}-\overline{y})^2,$$

$$\sigma_{xy} = \frac{1}{NM-1}\sum_{i=1}^{N}\sum_{j=1}^{M}(x_{ij}-\overline{x})(y_{ij}-\overline{y}).$$

The dynamic range of Q is $[-1, 1]$. The best value 1 is achieved if and only if $y_{ij} = x_{ij}$ for all $i = 1, 2, \ldots, N$ and $j = 1, 2, \ldots, M$. The quality index actually composed of three different factors: loss of correlation, luminance distortion, and contrast distortion. So the definition of Q can be rewritten as three components

$$Q = \frac{\sigma_{xy}}{\sigma_x\sigma_y}\cdot\frac{2\overline{x}\,\overline{y}}{\overline{x}^2+\overline{y}^2}\cdot\frac{2\sigma_x\sigma_y}{\sigma_x^2+\sigma_y^2} \tag{27}$$

The first component is the linear correlation coefficient between x and y, whose dynamic range is $[-1, 1]$. The second component measures how close the two mean values of x and y are, whose dynamic range is $[0, 1]$. The third component measures how similar the two variances of the images x and y are. Its range of value is $[0, 1]$. The quality index Q is a powerful parameter in image quality measurement [34]. It is sensitive to a lot of image distortion type such as blurring, JPEG compression, additive Gaussian Noise, contrast stretching and so on [35]. Of course, it is no problem to serve as the neural networks input. Fig. 9 shows the relationship between the quality index Q and the MTF of field and city images, which illustrates that the quality index Q and the MTF are related.

4.4.2. Quality index Q extraction

The quality index Q can characterize the deviation between the original image and the degraded image. It is a comparison parameter. Therefore, in order to extract the quality index Q, the a priori feature points need to be found in a remote sensing image. Benefit from the a priori feature points, the original image in a particular area can be deduced. Finally, using the deduced

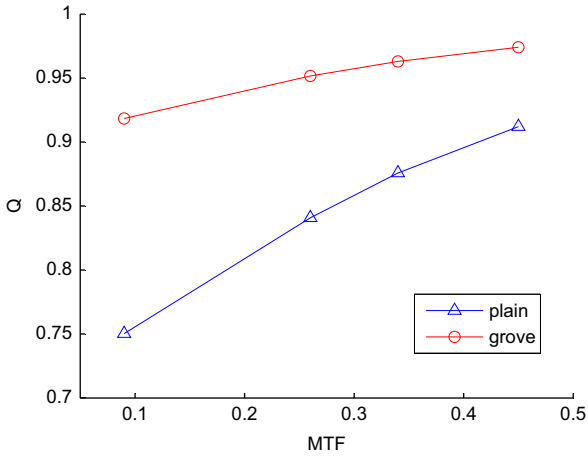

Fig. 9. Relationship between MTF and quality index Q of plain and grove images.

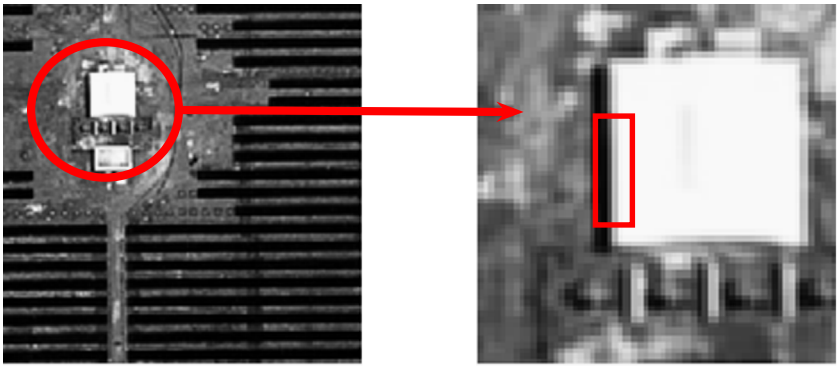

Fig. 10. Extraction quality index Q from an image.

original image and the actual image in a particular area the quality index Q can be extracted. As shown in Fig. 10, the high-contrast edge of a building can be used as a priori feature point. Using the a priori feature point, the original high-contrast edge in the rectangular area of size 14 pixels $\times$ 56 pixels can be inferred. Then the quality index Q of the image can be extracted from the rectangular area.

In practice, the high-contrast edge of a rectangular area can be used as a priori feature point, but it is not the only feature point, other a priori feature points which can help us to deduce the original image will be accepted. In addition, the image area used for extracting the quality index Q should keep the same size in a measurement work.

5. Neural networks and Markov model

5.1. The input vector of neural networks

The neural networks input vector V_{MTF} is composed of 9 components discussed above. The parameters of the input vector are linked to the MTF of images. Finally, the input vector can be

described as

$$V_{MTF} = \{variance, skewness, kurtosis, \gamma(1), \gamma(3), \gamma(5), \gamma(50), V(f_N), Q\}' \tag{28}$$

5.2. Neural networks algorithm and training

In our work, a neural networks is constructed to estimate the MTF of remote sensing images using the vector V_{MTF} as neural networks input. This neural network is a back propagation networks using Levenberg–Marquardt algorithm. It has one input layer, two hidden layers, and one output layer. The transfer function of the two hidden layers is hyperbolic tangent sigmoid function, and the output layer transfer function is Purelin function. The number of input layer nodes is 9, and the number of output layer nodes is 1. Meanwhile, the number of the hidden layer nodes should be designed and optimized. It is crucial for the performance of the neural networks to estimate the MTF of image taken by space optical camera.

In order to train the neural networks, 100 images with the size of 2000 pixels $\times$ 2000 pixels contained with different landscape structures are obtained from the remote sensing satellites GeoEye and WorldView. Each original image is simulated to images with different MTF at Nyquist frequency from 0.09 to 0.45 using the method mentioned in Section 3.2. The size of the simulated images is 500 pixels $\times$ 500 pixels. In order to alleviate the training difficulty, the input data of the neural networks is to be normalized between 0 and 1.

In practice, the initial number of the hidden layer nodes can be deduced from the geometric pyramid rule. For a neural network with input nodes n and output nodes m, the rule defines $r = \sqrt[3]{n/m}$, the first hidden layer nodes, initial value is mr^2, the second hidden layer nodes, initial value is mr. In our experiment, the initial input nodes $n=9$, output nodes $m=1$, the first hidden layer nodes is 5, and the second hidden layer nodes is 2. Then adjust the number of hidden layer nodes, until the network reaches to the satisfied training error 0.001. In the end, the first hidden layer nodes is 8, the second hidden layer nodes is 3. The curve of training error is shown in Fig. 11.

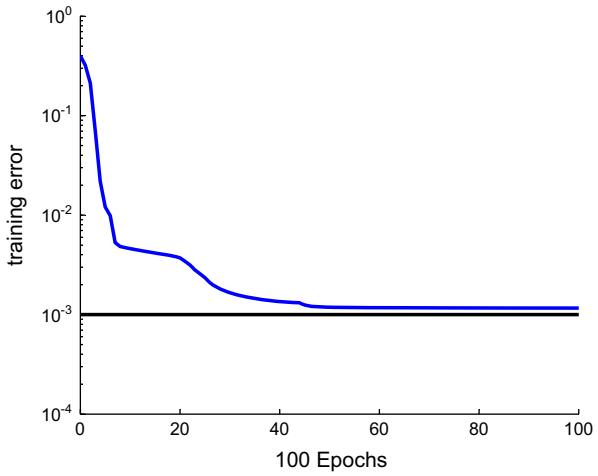

Fig. 11. The training error of the BP neural networks.

5.3. Markovian prediction model to correct the results

When using the trained neural networks to estimate the MTF of images at Nyquist frequency, the results will fluctuate at a certain range due to the neural networks cannot be trained perfectly. In order to correct the estimated results and improve the accuracy, the Markovian prediction model is applied in our work. The relative error sequence of estimated results can be written as δ_i, where $i=1,2,\ldots,n$. And then use the rule of golden section to divide the range of relative error into several error states. Next, use Markov transition matrix to characterize the transition relationship of error states. Finally, the new results estimated by trained neural networks can be further corrected by the Markovian prediction model.

The normalized relative error can be divided into several error states as follows:

$$\lambda_i = \Omega^q \overline{\delta}, \quad i=1,2,\ldots,n \tag{29}$$

where $\overline{\delta}$ is the mean of a relative error sequence δ_i, the ratio of golden section $\Omega \approx 0.618$, and q is an integer according to the scope of relative error to select.

6. Experiments

In order to verify the MTF estimation performance of the trained neural networks, an experiment is carried out. A test set which has 1110 images is build with the method mentioned in Section 3.2. The real MTF of the images in the test set is known in advance. In the experiment, we use the trained neural networks to estimate the MTF of images, and get the estimation results. Compare the estimation results with the real MTF of images we simulated, the relative error is used as a metric for the neural networks performance. The equation of relative error is as follows:

$$E_{error} = |M_{estimation} - M_{actual}| / M_{actual} \tag{30}$$

Using the trained neural networks to estimate the MTF of images with different landscape structures at Nyquist frequency, results show that the average relative error between the actual MTF and the estimated MTF is less than 9%, in the meanwhile, benefit from the Markovian prediction model, the results estimated by the neural networks can be further corrected, and make the average relative error narrow to 5%. The estimation average results and relative errors using BP neural networks and Markovian prediction model compared with only BP neural networks are presented in Table 1.

In the experiment there are some tips need to note:

(a) The image training sample set should have a representative, it needs to include all kinds of scenery types, such as images of town, city, plain, grove, desert and so on. And the number

Table 1
MTF estimation average results in column direction at Nyquist frequency and relative errors from more than 1000 images with different MTFs using trained BP artificial neural networks (ANNs) and via ANN and Markovian prediction model (ANN+MM), respectively.

Actual MTF	0.09	0.12	0.16	0.19	0.21	0.25	0.29	0.33	0.38	0.42
ANN	0.0781	0.1325	0.1463	0.2060	0.2250	0.2698	0.3158	0.3062	0.4099	0.4520
E_{error}	13.26%	10.23%	8.58%	8.41%	7.12%	7.90%	8.91%	7.21%	7.85%	7.62%
ANN+MM	0.0823	0.1279	0.1504	0.1981	0.2174	0.2610	0.3049	0.3187	0.3920	0.4351
E_{error}	8.52%	6.61 %	6.03%	4.28%	3.53%	4.40%	5.13%	3.42%	3.15%	3.59%

of images in the sample set should be greater than the number of the hidden layer nodes in ANN.

(b) It needs some time and patience to determine the number of hidden layer nodes of the ANN. If the number of the nodes is small it will be hard to resolve the complex problems. And if the number of the nodes is large it will increase the training time or make the ANN training hard.

(c) Since the ANN needs a lot of parameters extracted from images to estimate the MTF, too large image will make the computing inefficient. So in order to guarantee the estimation precision, the image taken by space optical camera should be segmented into the size same as the ANN training sample images. Use the ANN to estimate the MTF of every segmented images. The mean of the estimation MTFs can be the final result. In our work, the image size is 500 pixels $\times$ 500 pixels.

7. Conclusion

In this paper, a novel method to estimate the MTF of space optical camera from images via BP neural networks and Markov model is presented. Results show that the method is possible for any type of scenery taken by space optical camera. The main advantage of this method is that the MTF of space optical camera can be estimated only from the image taken by the camera without other equipment. It makes the MTF testing of space optical camera more flexible and convenient. Experiment results show that the average estimation relative error can further narrow to 5% via BP neural networks and Markovian prediction model, compared with 9% using only the BP neural networks. It can be envisaged that the results will be more accurate along with the more parameters sufficiently linked to the MTF of space optical camera to be found. We believe that these results will contribute to the development of the performance evaluation of space optical camera.

References

[1] G. Zhou, M. Kafatos, Future intelligent earth observing satellites, in: Proceedings of the Society of Photo-Optical Instrumentation Engineers (SPIE), vol. 5151, 2003, pp. 1–8.

[2] D. Williams, S. Goward, T. Arvidson, Landsat: yesterday, today, and tomorrow, Photogrammetric Engineering and Remote Sensing 72 (10) (2006) 1171–1178.

[3] M. Abolghasemi, D. Abbasi-Moghadam, Design and performance evaluation of the imaging payload for a remote sensing satellite, Optics and Laser Technology 44 (8) (2012) 2418–2426.

[4] P. Gastaldo, R. Zunino, I. Heynderickx, E. Vicario, Objective quality assessment of displayed images by using neural networks, Signal Processing: Image Communication 20 (7) (2005) 643–661.

[5] P. Le Callet, C. Viard-Gaudin, D. Barba, A convolutional neural network approach for objective video quality assessment, IEEE Transactions on Neural Networks 17 (5) (2006) 1316–1327.

[6] C. Charrier, O. Lzoray, G. Lebrun, Machine learning to design full-reference image quality assessment algorithm, Signal Processing: Image Communication 27 (3) (2012) 209–219.

[7] A. Braga, R. Schowengerdt, F. Rojas, S. Biggar, Calibration of the MODIS PFM SRCA for on-orbit, cross-track MTF measurement, Earth Observing Systems V (2000) 71–79.

[8] H. Hwang, Y. Choi, S. Kwak, M. Kim, W. Park, MTF assessment of high resolution satellite images using ISO 12233 slanted-edge method, in: Proceedings of SPIE, vol. 7109, pp. 710905-1–710905-9.

[9] J. Delvit, D. Lger, S. Roques, C. Valorge, Modulation transfer function and noise assessment, in: Geoscience and Remote Sensing Symposium, 2003, vol. 7, IEEE, pp. 4500–4502.

[10] J. Delvit, D. Leger, S. Roques, C. Valorge, Modulation transfer function and noise measurement using neural networks, in: Neural Networks for Signal Processing, 2003, IEEE, pp. 131–140.

[11] F. Viallefont-Robinet, D. Lger, Improvement of the edge method for on-orbit MTF measurement, Optics Express 18 (4) (2010) 3531–3545.
[12] P.B. Greer, T. van Doorn, Evaluation of an algorithm for the assessment of the MTF using an edge method, Medical Physics 27 (9) (2000) 2048–2059.
[13] U. Leloglu, E. Tunali, On-orbit modulation transfer function estimation for BiLSAT imagers, in: Proceedings of the ISPRS, 2006, pp. 45–51.
[14] L. Zhang, E.-K. Boukas, Stability and stabilization of Markovian jump linear systems with partly unknown transition probabilities, Automatica 45 (2) (2009) 463–468.
[15] L. Zhang, E.-K. Boukas, Mode-dependent filtering for discrete-time Markovian jump linear systems with partly unknown transition probabilities, Automatica 45 (6) (2009) 1462–1467.
[16] L. Zhang, J. Lam, Necessary and sufficient conditions for analysis and synthesis of Markov jump linear systems with incomplete transition descriptions, IEEE Transactions on Automatic Control 55 (7) (2010) 1695–1701.
[17] X. Zhao, L. Zhang, P. Shi, M. Liu, Stability and stabilization of switched linear systems with mode-dependent average dwell time, IEEE Transactions on Automatic Control 57 (7) (2012) 1809–1815.
[18] X. Zhao, Q. Zeng, Delay-dependent h-infinity performance analysis and filtering for Markovian jump systems with interval time-varying delays, International Journal of Adaptive Control and Signal Processing 24 (8) (2010) 633–642.
[19] X. Zhao, L. Zhang, P. Shi, M. Liu, Stability of switching positive linear systems with average dwell time switching, Automatica 48 (6) (2012) 1132–1137.
[20] X. Zhao, Q. Zeng, Stabilization of jump linear systems with mode-dependent time-varying delays, Optimal Control Applications and Methods 32 (2) (2011) 139–152.
[21] X. Zhao, Q. Zeng, New robust delay-dependent stability and h-infinity analysis for uncertain Markovian jump systems with time-varying delays, Journal of the Franklin Institute 347 (5) (2010) 863–874.
[22] L. Zhang, E.K. Boukas, J. Lam, Analysis and synthesis of Markov jump linear systems with time-varying delays and partially known transition probabilities, IEEE Transactions on Automatic Control 53 (10) (2008) 2458–2464.
[23] L. Zhang, Estimation for discrete-time piecewise homogeneous Markov jump linear systems, Automatica 45 (11) (2009) 2570–2576.
[24] B. Burke, P. Jorden, P. Vu, CCD technology, Experimental Astronomy 19 (2005) 69–102.
[25] J. Nieke, H. Schwarzer, A. Neumann, G. Zimmermann, Imaging spaceborne and airborne sensor systems in the beginning of the next century, in: Aerospace Remote Sensing'97, International Society for Optics and Photonics, 1997, pp. 581–592.
[26] G.C. Holst, CCD Arrays, Cameras, and Displays, SPIE-International Society for Optical Engine, 1998.
[27] T.S.L. Gerald, C. Holst, CMOS/CCD Sensors and Camera Systems, Society of Photo Optical, 2011.
[28] C. Latry, V. Despringre, C. Valorge, Automatic MTF measurement through a least square method, in: Remote Sensing, International Society for Optics and Photonics, 2004, pp. 233–244.
[29] J.-M. Delvit, D. Leger, S. Roques, C. Valorge, Modulation transfer function estimation from nonspecific images, Optical Engineering 43 (6) (2004) 1355–1365.
[30] C. Lo, A. Yeung, Concepts and Techniques of Geographic Information Systems, Prentice Hall, 2006.
[31] C.E. Woodcock, A.H. Strahler, D.L.B. Jupp, The use of variograms in remote sensing: I. Scene models and simulated images, Remote Sensing of Environment 25 (3) (1988) 323–348.
[32] G. Ramstein, M. Raffy, Analysis of the structure of radiometric remotely-sensed images, International Journal of Remote Sensing 10 (6) (1989) 1049–1073.
[33] M. Jung, D. Le, M. Gazalet, Univariant assessment of the quality of images, Journal of Electronic Imaging 11 (3) (2002) 354–364.
[34] A. Bouzerdoum, A. Havstad, A. Beghdadi, Image quality assessment using a neural network approach, in: Signal Processing and Information Technology, IEEE, 2004, pp. 330–333.
[35] W. Zhou, A.C. Bovik, A universal image quality index, IEEE Signal Processing Letters 9 (3) (2002) 81–84.